Stability of Water-Stable C_{60} Clusters to OH Radical Oxidation and Hydrated Electron Reduction

JAESANG LEE,[†] WEIHUA SONG,[‡] SEUNG S. JANG,[§] JOHN D. FORTNER,[||] PEDRO J. J. ALVAREZ,[†] WILLIAM J. COOPER,[‡] AND JAE-HONG KIM*,[⊥]

School of Civil and Environmental Engineering, and Department of Chemistry, Rice University, Houston, Texas 77005, Department of Civil and Environmental Engineering, University of California, Irvine, California 92697, and School of Materials Science and Engineering, and School of Civil and Environmental Engineering, Georgia Institute of Technology, Atlanta, Georgia 30332

Received November 23, 2009. Revised manuscript received April 1, 2010. Accepted April 5, 2010.

Reactions of water-stable C_{60} clusters (nC_{60}) in water with OH radicals (•OH) and hydrated electrons (e_{aq}^-), generated by steady-state γ-radiation, were observed and characterized. Ordered C_{60} clusters were relatively recalcitrant to highly reactive •OH and e_{aq}^- species, with only a fraction of carbons oxidized and reduced, respectively. Pulse radiolysis suggested that the reactions of nC_{60} with OH• and e_{aq}^- were diffusion limited, with rate constants of $(7.34 \pm 0.31) \times 10^9$ M^{-1} s^{-1} and $(2.34 \pm 0.02) \times 10^{10}$ M^{-1} s^{-1}, respectively. Quantum mechanical calculations of binding energy of the C_{60}—OH adduct as a function of C_{60} clustering degree indicate, despite an initial fast reaction, a slower overall conversion due to thermodynamic instability of C_{60}—OH intermediates. The results imply that ordered clustering of C_{60} in the aqueous phase significantly hinders C_{60}'s fundamental reactivity with radical species.

Introduction

Fate and transformation of C_{60} in the aqueous environment have received widespread research interest in the last several years. Since the earlier finding that hydrophobic C_{60} readily transforms into water-stable colloidal aggregates (often termed as nC_{60}) (*1*), research to date has examined the environmental implications of various properties of nC_{60} including photosensitization (*2*−*4*), colloidal stability and electrophoretic mobility (*5*−*7*), and toxicity (*8, 9*). Alternatively, some recent studies also showed that environmental conditions such as UV and sunlight irradiation (*10, 11*), presence of natural organic matter (*12, 13*), and exposure to oxidants such as ozone (*14*) also affect the chemical and physical properties of nC_{60} such that modified products would have significantly different impacts on the environment. Consequently, understanding the potential transformation of C_{60} in natural and engineered environments is a critical step toward understanding C_{60}'s ultimate fate in the environment.

Radical reactivity is one of the most fundamental chemical properties associated with contaminants of environmental concern. It is well-known that the spherical structure of C_{60} and resulting pyramidalization of the sp^2 carbons are responsible for the relatively high reactivity of C_{60} with various radicals at the carbon−carbon double bonds (*15, 16*). For example, C_{60} readily reacts with alkyl radicals to form stable nonradical intermediates (*15, 16*) as well as long-lived radical adducts (*17, 18*) that are available for further radical additions leading to multiple C_{60} alkylation (*15*). Reactions of C_{60} with other radicals such benzyl and halomethyl radicals were also found to be kinetically favorable (*19*−*21*). The exceptional radical reactivity of C_{60} cage carbons renders its functionalized derivatives susceptible to radical reactions as well (*22*−*25*). For example, effective quenching of reactive oxygen species (ROS) by functionalized C_{60} was demonstrated in biological systems (*23, 24*). Water-soluble C_{60} derivatives also exhibited diffusion-limited reaction with •OH (*22, 25*).

Despite extensive past research efforts evaluating fundamental reactivity of C_{60}, there is a still lack of understanding on underivatized C_{60}'s reaction with •OH, partly due to difficulty of performing kinetics studies on the •OH reaction in organic solvents and extremely low solubility of C_{60} in water. Past studies have postulated high reactivity of C_{60} with •OH based on the diffusion-limited bimolecular rate constant for other radical reactions (*22, 25*) and high radical scavenging capacity of water-soluble C_{60} derivatives (*23, 24*). Considering that •OH is ubiquitous in the environment (*26, 27*) and frequently used in engineered processes including water treatment (*28, 29*), it is important to understand the reaction of •OH with C_{60}, in particular in the form of nC_{60}, for evaluating C_{60}'s fate and transformation in the environment.

This study investigates the reaction of nC_{60} with •OH and e_{aq}^- in water. Steady-state γ-radiation under N_2- and N_2O-saturated conditions were performed along with detailed characterization of products using UV−vis absorption, XPS, ATR-FITR, and LDI-MS. Pulse radiolysis approximated the rate constants for oxidation and reduction reactions of nC_{60} with •OH and e_{aq}^-. The density functional theory (DFT) calculation was performed with C_{60} clusters (for the first time in the literature) to further explore the energistic status of transient radical adducts.

Experimental Section

Preparation of Aqueous Stable C_{60}. C_{60} clusters in water were prepared according to Fortner et al. (*1*). Briefly, THF containing 25 mg/L C_{60} (sublimed, 99.9%, Materials Electronics Research Corporation, Tucson, AZ) was purged with N_2, stirred overnight to reach saturation, and filtered through a 0.22 μm nylon membrane (Osmonics Corp). Ultrapure water (>18 MΩ) was added at a flow rate of 500 mL/min to an equal volume of the C_{60}−THF solution. THF was subsequently evaporated at 75−80 °C using a rotary evaporator to obtain a water suspension of nC_{60}. The suspension was further vacuum filtered through a 0.22 μm cellulose acetate membrane into a sterile container and stored in the dark. To ensure the elimination of residual organics (e.g., THF and THF oxidation byproducts (*30*)), the resultant concentrate was washed six times with ultrapure water using an ultrafiltration membrane with molecular weight cutoff of 10,000. The residual THF concentration in the final suspension was

* Corresponding author phone: (404) 894-2216; fax: (404) 385-7087; e-mail: jaehong.kim@ce.gatech.edu.
[†] School of Civil and Environmental Engineering, Rice University.
[‡] University of California, Irvine.
[§] School of Materials Science and Engineering, Georgia Institute of Technology.
[||] Department of Chemistry, Rice University.
[⊥] School of Civil and Environmental Engineering, Georgia Institute of Technology.

10.1021/es903550e

Published on Web 04/16/2010

SCHEME 1. Reaction of the C_{60} Aggregation Model with OH Radical: (a) single C_{60}; (b) one-layer system; (c) two-layer system; (d) three-layer system

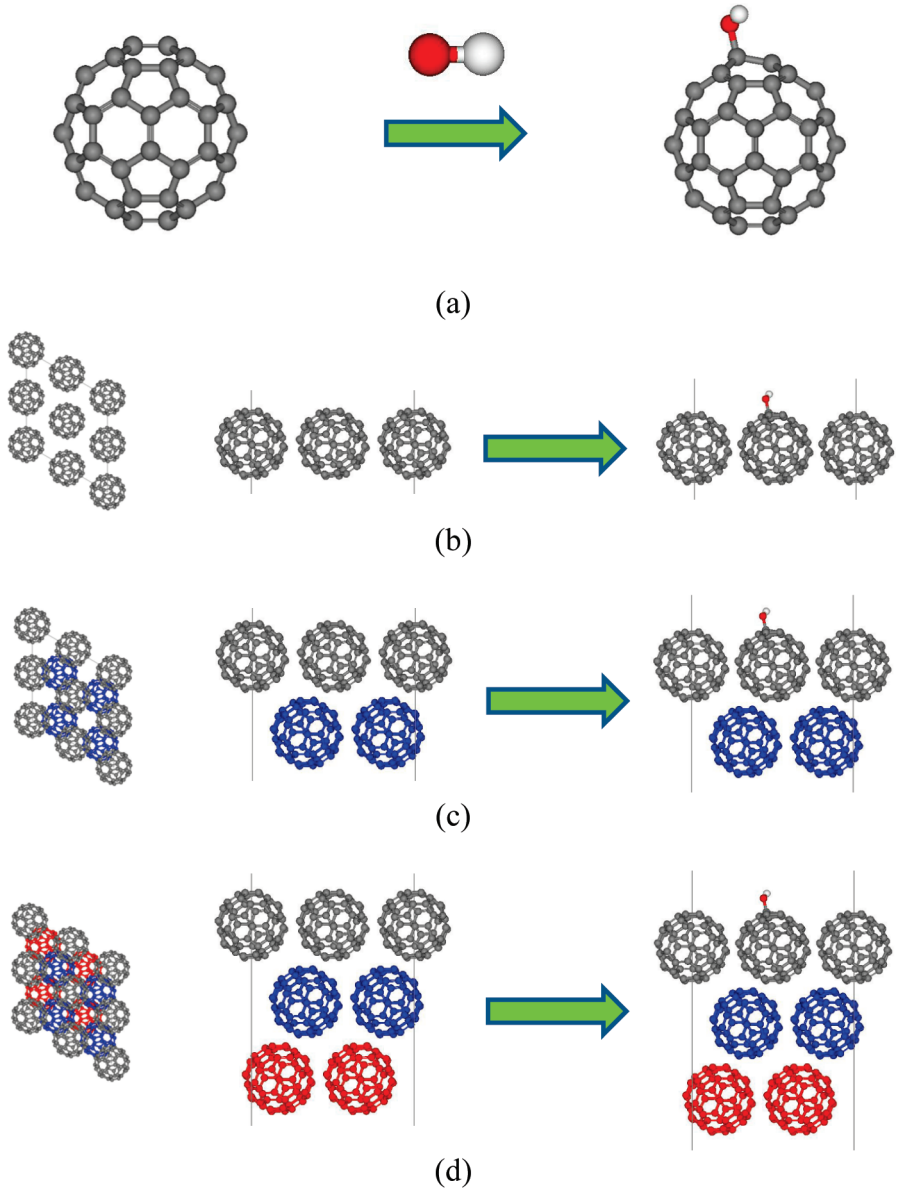

verified to be below the detection limit (10 ppb) of a GC-MS headspace analysis (Agilent model 6890 N gas chromatograph equipped with a Teledyne Tekmar HT3 headspace autosampler and a 30 m × 0.22 mm o.d. DB-5 ms column connected to an Agilent model 5974 inert mass-selective detector). Details on the physical and chemical characteristics of nC_{60} are available in our earlier work (*1*).

Gamma and Pulse Radiolysis. A Shepherd 109−86 Cobalt 60 source was used for steady-state γ-radiation at rate of 0.0722 kGy min^{-1} as measured by Fricke dosimetry. For selective production of •OH, the reaction solution (adjusted to pH 5.5) was first saturated with N_2O such that e_{aq}^- and •H resulting from H_2O radiolysis, in addition to •OH, is converted to •OH ($e^-_{aq} + N_2O + H_2O \rightarrow N_2 + HO^- + {}^{\bullet}OH$; $k_1 = 9.1 \times 10^9$ M^{-1} s^{-1} and $H^{\bullet} + N_2O \rightarrow {}^{\bullet}OH + N_2$; $k_2 = 2.1 \times 10^6$ M^{-1} s^{-1}) (*31*). For e_{aq}^- reaction, the solution was first purged with N_2 to remove dissolved O_2, and 0.10 M 2-propanol was added such that •OH and •H are scavenged as a stable 2-propanol radical ($(CH_3)_2CHOH + {}^{\bullet}OH \rightarrow (CH_3)_2C^{\bullet}OH + H_2O$; $k_3 = 1.9 \times 10^9$ M^{-1} s^{-1} and $(CH_3)_2CHOH + H^{\bullet} \rightarrow (CH_3)_2C^{\bullet}OH + H_2$; $k_4 = 7.4 \times 10^7$ M^{-1} s^{-1}) (*31*).

A 8-MeV Titan Beta model TBS-8/16-1S linear accelerator was used to examine the reaction kinetics. Details of the equipment are described elsewhere (*32*). The reaction solution was continuously purged with either N_2O (for •OH production) or N_2 (for e_{aq}^- production) during radiolysis. An average dose of 3 to 5 Gy per 2−3 ns pulse was measured by monitoring $SCN^{\bullet -}$ at $\lambda = 472$ nm ($G\varepsilon = 5.2 \times 10^{-4}$ m^2 J^{-1} where G [μmol J^{-1}] = the number of species per 100 eV and ε [M^{-1} cm^{-1}] = the molar absorptivity of $SCN^{\bullet -}$ at $\lambda = 472$ nm) (*33*) under N_2O-saturated conditions (1.00×10^{-2} M KSCN). The transient absorption spectra were monitored in the wavelength region from 250 to 600 nm. All data in the pulse radiolysis experiments were determined by averaging 8 to 12 replicate pulses using the continuous flow mode of the instrument.

Characterization. Samples for product characterization were obtained by continuous γ-radiation to 0.1 mM C_{60} suspension at a dose of 40 kGy under N_2O- or N_2-saturated conditions. X-ray photoelectron spectroscopy (XPS) analysis was carried out using a PHI Quanteria SXM scanning X-ray microprobe ULVAC-PHI with an Al mono, 24.8 WX- ray

source, and a 100.0 μm X-ray spot size at 45.0° (26.00 eV for 1 h). Samples were prepared by sputter-coating a clean silicon substrate with Au and then evaporating 100 μL of product solution on the substrate overnight at room temperature in a dust-free atmosphere. Data were analyzed with PeakFit to estimate peak position and relative peak areas. ATR-FTIR analysis was conducted using a Thermo Nicolet Nexus 870 FTIR spectrometer equipped with a Pike Technologies horizontal attenuated total reflectance (HATR) germanium trough. MS analyses via a laser desorption ionization (LDI) was performed using a tandem time-of-flight (TOF/TOF) mass spectrometer equipped with a 200 Hz laser (Applied Biosystems 4700 Proteomics Analyzer) under positive ion mode. For matrix-assisted (MALDI) analyses, samples were temporarily dried and dissolved into an organic matrix (cyano-4-hydroxycinnamic acid (CHCA)) for increased sensitivity toward less polar products.

Computational Methods. The face-centered cubic (FCC) crystal structure of C_{60} with $a = b = c = 14.052$ Å and $\alpha = \beta = \gamma = 90°$ (*34*) was selected as a model for the C_{60} cluster. As shown in Scheme 1, the C_{60} clustering phenomenon was simulated by placing layers of orderly packed C_{60} molecules in a vacuum. The geometry of the layered model was optimized through DMol3 (*35, 36*), quantum mechanics software, with the local density approximation (LDA) (*37*) and Perdew−Wang (PWC) functional (*38*). The all-electron calculations in DMol3 were performed on a medium integration grid with the spin unrestricted electronic wave functions in a double-numeric quality basis set (DN). The energy minimization was performed using the gamma point ($1 \times 1 \times 1$).

Results and Discussion

Reaction of C_{60} Clusters with •OH and e_{aq}^-. Figure 1 shows a gradual loss of characteristic peaks of nC_{60} (i.e., sharp absorption near 350 nm and broadband absorption near 450 nm) during γ-radiolysis, indicating molecular alteration due to reaction with •OH. The reaction was, however, extremely slow considering that this resulted from exposing 10 and 50 μM C_{60} colloid to the cumulative radiation of 20 and 40 kGy, corresponding to overall 11 and 22 mM •OH exposure. As a comparison, γ-radiation at a dose of only 0.25 kGy would lead to more than 99% oxidation of 10 mM phenol (*39*). Alternatively, experiments performed using TiO_2 photocatalysts to generate •OH under UVA irradiation (*40*) suggested that little UV spectral change was noticed with C_{60} clusters under the condition in which 0.1 mM 4-chlorophenol was completely degraded (see text S1 and Figure S1). These results suggest that nC_{60} is relatively resistant to •OH attack, and most advanced oxidation processes employed in water treatment would not readily achieve meaningful conversion. Similarly, C_{60} clusters slowly reacted with 20 and 40 kGy of γ-radiation under N_2-saturated conditions and in the presence of excess 2-propanol as an •OH scavenger, equivalent to overall e_{aq}^- exposure of 5.4 and 11.8 mM, respectively (Figure 2). Absorbance in the wavelength regions from 450 to 500 nm did not increase, indicating no cluster precipitation through electron-induced C_{60} polymerization (*41*). This observed stability of nC_{60} toward reactions with •OH and e_{aq}^- is consistent with earlier observations, albeit experimental conditions are not comparable (*41, 42*). For example, a trace amount of oligomers (less than 4% of initial C_{60} content) as polymerized products was found to form during γ-radiation of 70 μM C_{60} clusters at an impractically high dose exceeding 6 MGy (*41*), and 6 μM C_{60} clusters were not degraded by Co-radiation at 33 kGy (*42*).

Product Characterization. XPS spectra of γ-radiolysis product (i.e., 40 kGy under either N_2O- or N_2-saturated conditions) in Figure 3a suggest that only ca. 36% of C_{60} carbons at the surface converted to monooxidized forms (at

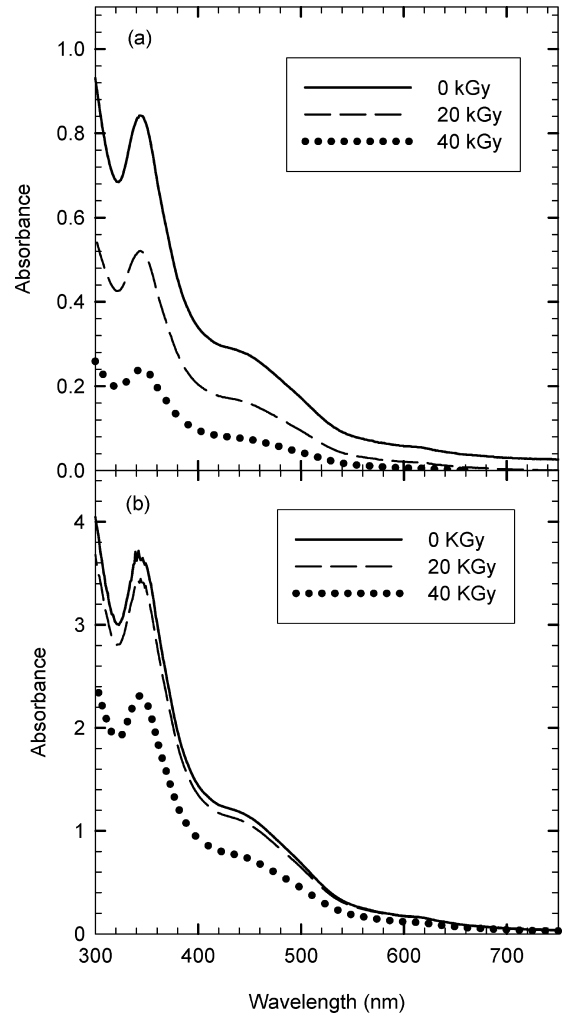

FIGURE 1. UV−vis absorption spectra changes of C_{60} clusters at a concentration of (a) 10 μM and (b) 50 μM under N_2O-saturated conditions with steady-state γ-radiation time (pH_i = 5.5).

287.65 eV) despite the high concentration ratio of $[•OH]_{total}/[C_{60}]_0 = 220$. Note that this ratio is underestimated, as only C_{60} molecules at the cluster surface are available for the reaction. In marked contrast to ozonolysis (*14*) or UVC photolysis (*11*), in which a large amount of carbons are dioxigenated to carbonyl, carboxylic, and hemiketal functionalities, little further oxidation was observed. Figure 3b demonstrates that ca. 42% of surface carbons reductively transformed to hydrogenated carbons (C−H, at 283.52 eV) via exposure to an excessive amount (11.8 mM) of e_{aq}^-. Qualitative MS analyses (data not shown) for both reactions support XPS observations, indicating (partial and mixed) fullerene derivatization observed as a mixture of higher molecular weight derivatives compared to the parent C_{60}. Additionally, a relatively high 720 m/z signal is observed in all samples, indicating that the underivatized C_{60} cage architecture remains either as unmodified C_{60} and/or as derivatives which lose functionality during LDI, resulting in a parent signal, which has been observed previously (*14*). ATR-FTIR analyses (data not shown) support functional derivatization, in which both reduced and oxidized carbons for these reactions are indicated by IR peaks at 3400 (broad), 2980, 2920, 1725, 1440, 1275, 1190, 1100, 1010, 950, 800, 730 cm^{-1} with varying peak intensities depending on oxidation versus reduction.

Reaction Kinetics. A series of transient differential absorption spectra with $\lambda_{max} = 280$ nm, indicative of the

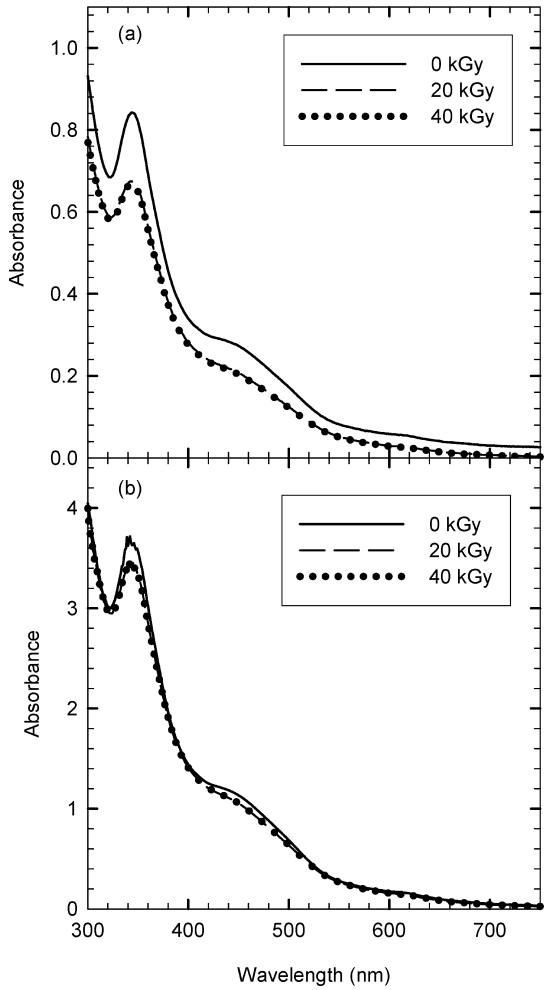

FIGURE 2. UV−vis absorption spectra changes of C_{60} clusters at a concentration of (a) 10 μM and (b) 50 μM under N_2-saturated conditions with steady-state γ-radiation time (pH_i = 5.5).

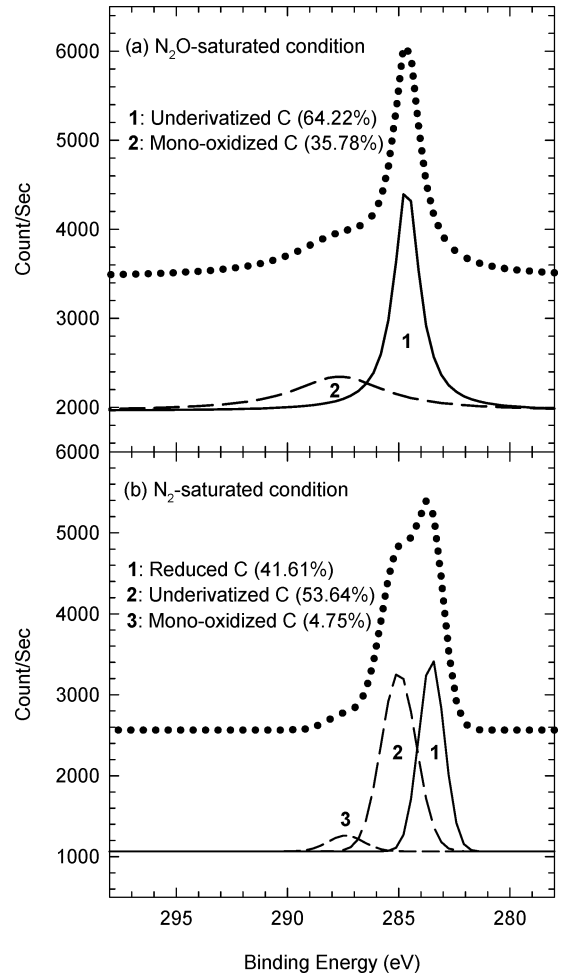

FIGURE 3. C(1s) XPS spectrum and curve-fitting analysis of products generated after the 40 kGy Co-radiation of C_{60} clusters in water with (a) N_2O- and (b) N_2-saturation. Top: Points represent spectral data. Bottom: Curve-fitting deconvolution expressed in relative intensity (Gaussian fits).

formation of C_{60}−OH radical adducts, was monitored after the radiation of pulsed electron beams to N_2O-saturated nC_{60} suspensions (Figure S2). However, the spectral intensity was too weak to derive a rate constant, while monitoring the decay of 280 nm absorption indicated rapid loss of intermediate species within approximately 100 μs. Alternatively, the following competition kinetics approach using SCN^- was employed:

$$\bullet OH + C_{60} \xrightarrow{k_5} \text{intermediate} \quad (1)$$

$$\bullet OH + SCN^- (+ SCN^-) \xrightarrow{k_6} OH^- + (SCN)_2^{\bullet -} \quad (2)$$

Assuming all the carbons in nC_{60} participate in the reaction with •OH, the following equation is derived:

$$\frac{[(SCN)_2^{\bullet -}]_0}{[(SCN)_2^{\bullet -}]} = 1 + \frac{k_5[C_{60}]}{k_6[SCN^-]} \quad (3)$$

where $[(SCN)_2^{\bullet -}]_0$ indicates the concentration of $(SCN)_2^{\bullet -}$ when C_{60} is absent, and $[(SCN)_2^{\bullet -}]$ is the concentration of $(SCN)_2^{\bullet -}$ when C_{60} coexists with SCN^-. Note that the reduction of nC_{60} by $(SCN)_2^{\bullet -}$ is not thermodynamically feasible, as $E((SCN)_2^{\bullet -}/2SCN^-) = +1.31$ V_{NHE} (*43*) and $E^0(C_{60}/C_{60}^{\bullet -}) = -0.2$ V_{NHE} (*44*). Control experiments also confirmed that the kinetics of $(SCN)_2^{\bullet -}$ decay was not affected by the addition of nC_{60} (data not shown). Figure 4 shows that absorption intensity of $(SCN)_2^{\bullet -}$ at λ_{max} = 472 nm became gradually reduced as nC_{60} concentration increased, implying competitive involvement of nC_{60} in •OH reaction with SCN^-. A plot of eq 3 ($[(SCN)_2^{\bullet -}]_0/[(SCN)_2^{\bullet -}]$ vs $[C_{60}]/[SCN^-]$) shows a linear correlation with a slope of k_5/k_6 (inset of Figure 4). Using k_6 ($\bullet OH + SCN^-$) = 1.05×10^{10} M^{-1} s^{-1}, the rate constant for the •OH reaction with nC_{60} was calculated as $k_5 = (7.34 \pm 0.31) \times 10^9$ M^{-1} s^{-1}.

The rate constant for e_{aq}^- reaction with nC_{60} was measured by directly monitoring the absorption of e_{aq}^- at 700 nm. A series of e_{aq}^- decay curves at different C_{60} concentrations in Figure 5 indicates that the rate of e_{aq}^- consumption by nC_{60} gradually increased with C_{60} concentration. The decay profiles were fitted to pseudo-first-order kinetics, and the second-order rate constant for the reaction between e_{aq}^- and nC_{60} was determined to be $(2.34 \pm 0.02) \times 10^{10}$ M^{-1} s^{-1} (inset of Figure 5).

The measured rate constants suggested diffusion-limited reaction kinetics for •OH and e_{aq}^- with nC_{60} in water. Because only C_{60} molecules at the cluster surface are available for the reaction, which constitute 2 to 8% of the total C_{60}, assuming that the average size of nC_{60} is approximately 100 nm and nC_{60} is spherical (*1*−*4*), the actual rate constant between •OH and e_{aq}^- with C_{60} should be at least 1 to 2 orders of magnitude higher than that measured above. This is consistent with the estimated high susceptibility of C_{60} carbon to •OH oxidation (*22*) or e_{aq}^- reduction (*45*), i.e., calculated based on the

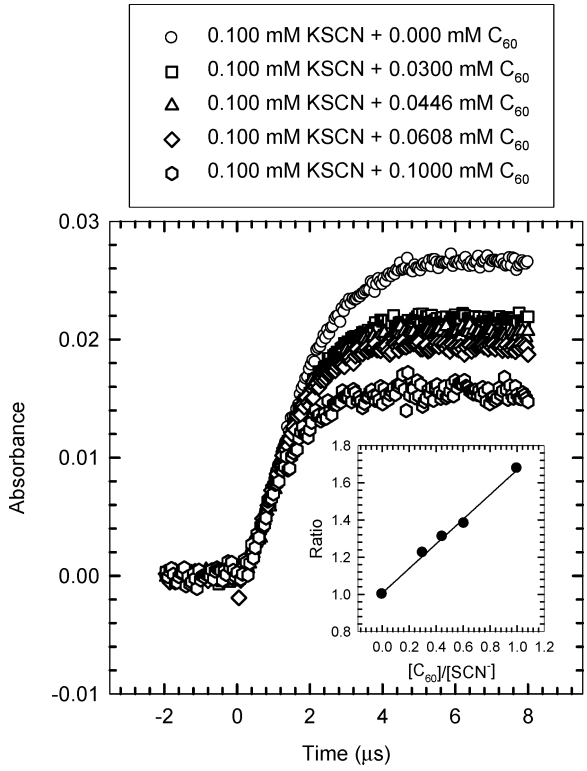

FIGURE 4. Growth kinetics of $(SCN)_2^{\bullet-}$ monitored at 472 nm in the absence and presence of nC_{60} at various concentrations under N_2O-staturated conditions. Inset: Competitive kinetics plot for the reaction between C_{60} clusters and OH radical using SCN^- as a standard ($[SCN^-]_0 = 0.1$ mM).

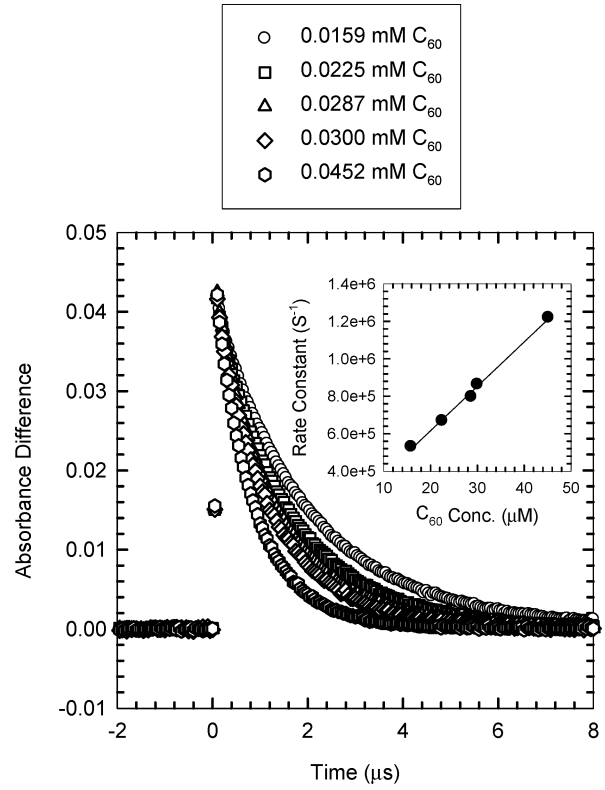

FIGURE 5. Decay kinetics of hydrated electron monitored at 700 nm in presence of nC_{60} at various concentrations under N_2-staturated conditions. Excess concentration of 2-propanol was applied to completely scavenge OH radicals and hydrogen atoms. Inset: Second-order linear plot for determination of the rate constant for reduction of nC_{60} with hydrated electrons ($[2\text{-propanol}]_0 = 0.1$ M).

reactivity of a homologous series of functionalized C_{60}. However, this is somewhat contradictory to the above γ-radiolysis study in which C_{60} transformation was severely limited even after exposure to an exceedingly excessive amount of •OH and e_{aq}^-. Because such slow kinetics are not limited by initial reactions of •OH and e_{aq}^- with nC_{60}, it is plausible to assume thermodynamic instability of the transient adducts and consequential unavailability for the subsequent reactions.

DFT Calculations. The DFT calculation on the binding energy (BE) of the C_{60}−OH radical adduct as a function of C_{60} aggregation degree was performed using the layered model that simulates the C_{60} clustering phenomenon (Scheme 1). Although the C_{60} clustering will include some extent of randomness in surface structure, it is expected that the development of overall structure will proceed to have more ordered structure with increasing cluster size, which is energetically favorable. Table 1 summarizes the lowest unoccupied molecular orbital (LUMO), the highest occupied molecular orbital (HOMO)), and HOMO−LUMO energy gap (E(LUMO − HOMO)) of C_{60} and the C_{60}−OH radical adduct for each layered system. The increase in the system dimension (further C_{60} clustering) results in reduction in E(LUMO − HOMO) of C_{60} (Table 1); i.e., the electronic structure of the C_{60} cluster is developed toward that of the bulk solid phase with an increasing number of layers. This result is compatible

TABLE 1. DFT Calculations on Energistic Status of C_{60} and C_{60}−OH Radical Adduct

system	energy (Ha)	E(HOMO) (eV)	E(LUMO) (eV)	E(LUMO−HOMO) (eV)
hydroxyl radical (•OH)	−75.140423	−6.683	−0.599	6.084
single C_{60}				
C_{60}	−2263.053334	−9.345	−7.770	1.575
$\bullet C_{60}$−OH	−2338.26528	−8.565	−8.252	0.313
binding energy (kcal/mol)	−44.88			
one-layer system				
C_{60} (one-layer)	−9052.518756	−8.889	−7.895	0.994
$\bullet C_{60}$ (one-layer)−OH	−9127.73045	−8.555	−8.283	0.272
binding energy (kcal/mol)	−44.72			
two-layer system				
C_{60} (two-layer)	−18105.151913	−8.786	−7.879	0.907
$\bullet C_{60}$ (two-layer)−OH	−18180.31979	−8.462	−8.185	0.277
binding energy (kcal/mol)	−17.23			
three-layer system				
C_{60} (three-layer)	−27158.03253	−8.589	−7.807	0.782
$\bullet C_{60}$ (three-layer)−OH	−27233.09109	−8.289	−8.011	0.278
binding energy (kcal/mol)	51.37			

with the empirical observation that the progress in C_{60} clustering rendered the UV−vis spectra of C_{60} more red-shifted (*3*). As a result, *E*(LUMO − HOMO) as a function of C_{60} aggregation suggests that the dimensional expansion of the layered model in our DFT calculation can reflect the effect of C_{60} clustering on the reaction of C_{60} with •OH.

Table 1 shows the change in BE of C_{60} and •OH (eq 4) with the development of C_{60} layered structure, indicative of the effect of C_{60} aggregation on energetic status of the radical adduct.

$$\Delta E_{\text{reaction}} = E(\bullet C_{60}\text{−OH}) - [E(C_{60}) + E(\bullet\text{OH})] \qquad (4)$$

As shown in Table 1, the DFT BE is positively increased as the number of layers is increased: −44.88 kcal/mol for a single C_{60} molecule; −44.72 kcal/mol for C_{60} in one-layer; −17.23 kcal/mol in two-layer; 51.37 kcal/mol in three-layer. The results demonstrate that the formation of the OH radical adduct with C_{60} became thermodynamically less favorable as the C_{60} cluster model was further developed. Consequently, the destabilization of the C_{60}−OH radical adduct with further C_{60} clustering can be responsible for the extremely low efficacy in oxidative degradation of C_{60} clusters with •OH. Further understanding of the reaction energetics for •OH oxidation of C_{60} clusters and the reaction involving e_{aq}^- requires in-depth investigation with incorporation of additional influential parameters (e.g., other possible reaction pathways and energy barriers among multiple transient states) to the DFT calculation.

The above results collectively suggest the relative recalcitrance of nC_{60} against •OH oxidation and e_{aq}^- reduction. In contrast, the kinetic measurements with pulse radiolysis indicate that nC_{60} reactions with •OH and e_{aq}^- proceed with diffusion-limited rate constants. The DFT calculations on the BE of C_{60}−OH radical adducts with the layer simulation model suggest that further conversion of the transient radical adducts to oxidation product(s) becomes thermodynamically less favorable as C_{60} aggregation proceeds. Consequently, in natural and engineered environments, chemical transformations of nC_{60} by •OH and e_{aq}^- are most likely very limited. These findings further suggest that the reactivity of C_{60} as aggregates in water significantly differs from that of dissolved C_{60} in an organic phase because of the unique clustering phenomena in water. Therefore, the environmental fate of nC_{60} due to these reactions should not be postulated based on the properties of pristine C_{60} in different media.

Acknowledgments

This work was funded by the United States Environmental Protection Agency (USEPA) STAR Grant #D832526 and also partially funded by the National Science Foundation (Grants R3B520-722000 and EEC-0647452). Radiolysis experiments were performed at Radiation Laboratory, University of Notre Dame. The authors thank David Bostwick at the Mass Spectroscopy Facilities at Department of Chemistry and Biochemistry, Georgia Institute of Technology, for MS analyses; Adina Boyd at the Department of Chemistry, Rice University, for XPS analysis; and Brandon Lafferty at Department of Soil Chemistry, University of Delaware, for ATR-FTIR analysis and discussion.

Supporting Information Available

Additional information as noted in the text. This material is available free of charge via the Internet at http://pubs.acs.org.

Literature Cited

(1) Fortner, J. D.; Lyon, D. Y.; Sayes, C. M.; Boyd, A. M.; Falkner, J. C.; Hotze, E. M.; Alemany, L. B.; Tao, Y. J.; Guo, W.; Ausman, K. D.; Colvin, V. L.; Hughes, J. B. C_{60} in water: Nanocrystal formation and microbial response. *Environ. Sci. Technol.* **2005**, *39*, 4307–4316.

(2) Lee, J.; Fortner, J. D.; Hughes, J. B.; Kim, J. H. Photochemical production of reactive oxygen species by C_{60} in the aqueous phase during UV irradiation. *Environ. Sci. Technol.* **2007**, *41*, 2529–2535.

(3) Lee, J.; Kim, J. H. Effect of encapsulating agents on dispersion status and photochemical reactivity of C_{60} in the aqueous phase. *Environ. Sci. Technol.* **2008**, *42*, 1552–1557.

(4) Lee, J.; Yamakoshi, Y.; Hughes, J. B.; Kim, J. H. Mechanism of C_{60} photoreactivity in water: Fate of triplet state and radical anion and production of reactive oxygen species. *Environ. Sci. Technol.* **2008**, *42*, 3459–3464.

(5) Brant, J.; Lecoanet, H.; Hotze, M.; Wiesner, M. Comparison of electrokinetic properties of colloidal fullerenes (nC_{60}) formed using two procedures. *Environ. Sci. Technol.* **2005**, *39*, 6343–6351.

(6) Chen, K. L.; Elimelech, M. Aggregation and deposition kinetics of fullerene (C_{60}) nanoparticles. *Langmuir* **2006**, *22*, 10994–11001.

(7) Chen, K. L.; Elimelech, M. Relating colloidal stability of fullerene (C_{60}) nanoparticles to nanoparticle charge and electrokinetic roperties. *Environ. Sci. Technol.* **2009**, *43*, 7270–7276.

(8) Colvin, V. L. The potential environmental impact of engineered nanomaterials. *Nat. Biotechnol.* **2003**, *21*, 1166–1170.

(9) Lyon, D. Y.; Brunet, L.; Hinkal, G. W.; Wiesner, M. R.; Alvarez, P. J. J. Antibacterial activity of fullerene water suspensions (nC_{60}) is not due to ROS-mediated damage. *Nano Lett.* **2008**, *8*, 1539–1543.

(10) Hou, W. C.; Jafvert, C. T. Photochemical transformation of aqueous C_{60} clusters in sunlight. *Environ. Sci. Technol.* **2009**, *43*, 362–367.

(11) Lee, J.; Cho, M.; Fortner, J. D.; Hughes, J. B.; Kim, J. H. Transformation of aggregate C_{60} in the aqueous phase by UV irradiation. *Environ. Sci. Technol.* **2009**, *43*, 4878–4883.

(12) Chen, K. L.; Elimelech, M. Interaction of fullerene (C_{60}) nanoparticles with humic acid and alginate coated silica surfaces: Measurements, mechanisms, and environmental implications. *Environ. Sci. Technol.* **2008**, *42*, 7607–7614.

(13) Li, Q. L.; Xie, B.; Hwang, Y. S.; Xu, Y. J. Kinetics of C_{60} fullerene dispersion in water enhanced by natural organic matter and sunlight. *Environ. Sci. Technol.* **2009**, *43*, 3574–3579.

(14) Fortner, J. D.; Kim, D. I.; Boyd, A. M.; Falkner, J. C.; Moran, S.; Colvin, V. L.; Hughes, J. B.; Kim, J. H. Reaction of water-stable C_{60} aggregates with ozone. *Environ. Sci. Technol.* **2007**, *41*, 7497–7502.

(15) Krusic, P. J.; Wasserman, E.; Keizer, P. N.; Morton, J. R.; Preston, K. F. Radical reactions of C_{60}. *Science* **1991**, *254*, 1183–1185.

(16) Mcewen, C. N.; Mckay, R. G.; Larsen, B. S. C_{60} as a Radical Sponge. *J. Am. Chem. Soc.* **1992**, *114*, 4412–4414.

(17) Krusic, P. J.; Wasserman, E.; Parkinson, B. A.; Malone, B.; Holler, E. R.; Keizer, P. N.; Morton, J. R.; Preston, K. F. Electron spin resonance study of the radical reactivity of C_{60}. *J. Am. Chem. Soc.* **1991**, *113*, 6274–6275.

(18) Morton, J. R.; Preston, K. F.; Krusic, P. J.; Hill, S. A.; Wasserman, E. ESR studies of the reaction of alkyl radicals with C_{60}. *J. Phys. Chem.* **1992**, *96*, 3576–3578.

(19) Dimitrijevic, N. M. Reaction of trichloromethyl and trichloromethylperoxyl radicals with C_{60} - a Pulse radiolysis study. *Chem. Phys. Lett.* **1992**, *194*, 457–460.

(20) Dimitrijevic, N. M.; Kamat, P. V.; Fessenden, R. W. Radical adducts of fullerenes C_{60} and C_{70} studied by laser flash photolysis and pulse radiolysis. *J. Phys. Chem.* **1993**, *97*, 615–618.

(21) Guldi, D. M.; Hungerbuhler, H.; Janata, E.; Asmus, K. D. Radical-Induced redox and addition-reactions with C_{60} studied by pulse radiolysis. *J. Chem. Soc., Chem. Commun.* **1993**, 84–86.

(22) Guldi, D. M.; Asmus, K. D. Activity of water-soluble fullerenes towards OH radicals and molecular oxygen. *Radiat. Phys. Chem.* **1999**, *56*, 449–456.

(23) Wang, I. C.; Tai, L. A.; Lee, D. D.; Kanakamma, P. P.; Shen, C. K. F.; Luh, T. Y.; Cheng, C. H.; Hwang, K. C. C_{60} and water-soluble fullerene derivatives as antioxidants against radical-initiated lipid peroxidation. *J. Med. Chem.* **1999**, *42*, 4614–4620.

(24) Foley, S.; Curtis, A. D. M.; Hirsch, A.; Brettreich, M.; Pelegrin, A.; Seta, P.; Larroque, C. Interaction of a water soluble fullerene derivative with reactive oxygen species and model enzymatic systems. *Fullerenes Nanotubes Carbon Nanostruct.* **2002**, *10*, 49–67.

(25) Lu, C. Y.; Yao, S. D.; Lin, W. Z.; Wang, W. F.; Lin, N. Y.; Tong, Y. P.; Rong, T. W. Studies on the fullerol of C_{60} in aqueous solution with laser photolysis and pulse radiolysis. *Radiat. Phys. Chem.* **1998**, *53*, 137–143.

(26) Zepp, R. G.; Faust, B. C.; Hoigne, J. Hydroxyl radical formation in aqueous reactions (Ph 3−8) of iron(II) with hydrogen peroxide - the photo-Fenton reaction. *Environ. Sci. Technol.* **1992**, *26*, 313–319.
(27) Zepp, R. G.; Hoigne, J.; Bader, H. Nitrate-induced photooxidation of trace organic chemicals in water. *Environ. Sci. Technol.* **1987**, *21*, 443–450.
(28) Legrini, O.; Oliveros, E.; Braun, A. M. Photochemical processes for water treatment. *Chem. Rev.* **1993**, *93*, 671–698.
(29) Pignatello, J. J.; Oliveros, E.; MacKay, A. Advanced oxidation processes for organic contaminant destruction based on the Fenton reaction and related chemistry. *Crit. Rev. Environ. Sci. Technol.* **2006**, *36*, 1–84.
(30) Zhang, B.; Cho, M.; Fortner, J. D.; Lee, J.; Huang, C. H.; Hughes, J. B.; Kim, J. H. Delineating oxidative processes of aqueous C_{60} preparations: Role of THF peroxide. *Environ. Sci. Technol.* **2009**, *43*, 108–113.
(31) Buxton, G. V.; Greenstock, C. L.; Helman, W. P.; Ross, A. B. Critical review of rate constants for reactions of hydrated electrons, hydrogen atoms and hydroxyl radicals ($OH^{\bullet}/O^{\bullet-}$) in aqueous solution. *J. Phys. Chem. Ref. Data* **1988**, *17*, 513–886.
(32) Asmus, K. D. Pulse-radiolysis methodology. *Methods Enzymol.* **1984**, *105*, 167–178.
(33) Buxton, G. V.; Stuart, C. R. Reevaluation of the thiocyanate dosimeter for pulse-radiolysis. *J. Chem. Soc., Faraday Trans.* **1995**, *91*, 279–281.
(34) Liu, S. Z.; Lu, Y. J.; Kappes, M. M.; Ibers, J. A. The Structure of the C_{60} Molecule - X-Ray Crystal-Structure Determination of a Twin at 110-K. *Science* **1991**, *254*, 408–410.
(35) Delley, B. AN all-electron numerical-method for solving the local density functional for polyatomic-molecules. *J. Chem. Phys.* **1990**, *92*, 508–517.
(36) Delley, B. From molecules to solids with the DMol(3) approach. *J. Chem. Phys.* **2000**, *113*, 7756–7764.
(37) Koch, W.; Holthausen, M. C., *A Chemist's Guide to Density Functional Theory*; Wiley-VCH: Weinheim, 2001.
(38) Perdew, J. P.; Wang, Y. Accurate and simple analytic representation of the electron-gas correlation-energy. *Phys. Rev. B* **1992**, *45*, 13244–13249.
(39) Lin, K. J.; Cooper, W. J.; Nickelsen, M. G.; Kurucz, C. N.; Waite, T. D. Decomposition of aqueous solutions of phenol using high energy electron beam irradiation - A large scale study. *Appl. Radiat. Isot.* **1995**, *46*, 1307–1316.
(40) Hoffmann, M. R.; Martin, S. T.; Choi, W. Y.; Bahnemann, D. W. Environmental applications of semiconductor photocatalysis. *Chem. Rev.* **1995**, *95*, 69–96.
(41) Albarran, G.; Basiuk, V. A.; Basiuk, E. V.; Saniger, J. M. Stability of interstellar fullerenes under high-dose *r*-irradiation. *Adv. Space Res.* **2004**, *33*, 72–75.
(42) Isakovic, A.; Markovic, Z.; Nikolic, N.; Todorovic-Markovic, B.; Vranjes-Djuric, S.; Harhaji, L.; Raicevi, N.; Romcevic, N.; Vasiljevic-Radovic, D.; Dramicanin, M.; Trajkovic, V. Inactivation of nanocrystalline C_{60} cytotoxicity by *r*-irradiation. *Biomaterials* **2006**, *27*, 5049–5058.
(43) Alfassi, Z., B.; Harriman, A.; Huie, R. E.; Mosseri, S.; Neta, P. The redox potenital of the azide/azidyl couple. *J. Phys. Chem.* **1987**, *91*, 2120–2122.
(44) Kamat, P. V.; Haria, M.; Hotchandani, S. C_{60} cluster as an electron shuttle in a Ru(II)-polypyridyl sensitizer-based photochemical solar cell. *J. Phys. Chem. B* **2004**, *108*, 5166–5170.
(45) Dimitrijevic, N. M.; Kamat, P. V. Excited state behavior and one-electron reduction of C_{60} in aqueous *r*-cyclodextrin solution. *J. Phys. Chem.* **1993**, *97*, 7623–7626.

ES903550E